ChemCatChem

Research Article
doi.org/10.1002/cctc.202401106

Chemistry Europe
European Chemical Societies Publishing

www.chemcatchem.org

Epoxidation at Isolated Titanium Site Modeled by Ti-Siloxy-Polyoxometalates Built on $[\alpha\text{–A–}XW_9O_{34}]^{n-}$ and $[\alpha\text{–B–}YW_9O_{33}]^{9-}$: Comparative Study of Their Hydrolytic Stability

Ludivine K/Bidi,[a] Albert Solé-Daura,[b] Teng Zhang,[a] Alix Desjonquères,[a] Josep M. Poblet,[b] Anna Proust,[a] Jorge J. Carbó,*[b] and Geoffroy Guillemot*[a]

This report investigates the structural differences in a series of titanium complexes constructed from silanol functionalized polyoxometalate (*Silox*POMs) derivatives, designed to create a constrained coordination site for titanium (IV) cations, namely $(THA)_3[PW_9O_{34}(t\text{BuSiO})_3\text{Ti}(O\text{i}\text{Pr})]$ and $(THA)_3[SbW_9O_{33}(t\text{BuSiO})_3\text{Ti}(O\text{i}\text{Pr})]$. The complexes serve as structural and functional models for titanium silicates, facilitating the epoxidation of allylic alcohols and alkenes by aqueous hydrogen peroxide solutions. The different activity and selectivity observed between the two derivatives are attributed to variations in the polyoxotungstic platform used, A-type–$[XW_9O_{34}]^{n-}$ versus B-type –$[YW_9O_{33}]^{3-}$. A combined experimental and theoretical investigation highlights the influence of these structural differences on water interaction and hydrolytic stability, with A-type structures proving more susceptible to hydrolysis. In addition, the study also delves into the nuclearity of the active sites, a monomeric titanium (IV)-hydroperoxide [Ti]–(OOH) active species evidenced by diffusion NMR spectroscopy, and the influence of the presence of water on catalytic performance in epoxidation reaction, thus shedding light on the relationship between catalyst stability, intermediates formed and reaction pathway. The study finally demonstrates the suitability of B-type *Silox*POM derivatives as models for titanium silicates, offering insights into their stability and catalytic activity for epoxidation reactions.

1. Introduction

Partial oxidation represents the most important technology for the conversion of olefin feedstocks to higher valued synthons for industrial organic chemicals.[1–3] Although catalytic oxidation with dioxygen is highly desirable, successful applications are often restricted to the manufacturing of bulk petrochemicals due to the lack of control of the reaction selectivity when producing radicals in the media. In this context, hydrogen peroxide also appears as one of the most desirable oxidants.[4] Containing a high level of active oxygen and generating water as its only by-product, hydrogen peroxide is not very reactive with organic products but produces reactive forms in contact with metal catalysts.[5] Used as an aqueous solution, hydrogen peroxide has found wide use in catalytic oxidation of organic substrates using complexes of first row middle transition metals, such as iron and manganese, through the formation of high-valent intermediates.[6,7] In the case of oxophilic early transition metals such as titanium the use of aqueous hydrogen peroxide is less straightforward, probably due to the nature of the ligands involved, often alkoxides, and the high level of hydrolysis of the designed complexes. A major successful example is the enantioselective epoxidation of alkenes, a long-standing problem in homogeneous catalysis, first reported by Katsuki in 2005 using salalen-based titanium complexes, and then efficiently developed by H. J. Berkessel in 2013.[8–11] Although there are several outstanding results, most of the titanium-based catalysts require anhydrous conditions or hydrophobic environments and the preferred use of organic hydroperoxides as oxidants.[12]

In this context, the development of titanium-silicalite (TS1–MFI framework) materials in the mid-1980s by Enichem resulted in the emergence of effective and versatile heterogeneous catalysts for the liquid-phase oxidation of organic compounds with aqueous H_2O_2, for example olefin epoxidation, alcohol oxidation, phenol hydroxylation and ketone ammoximation.[5,13–17] Titanium silicates are at the heart of two important technologies for the production of propylene oxide from propylene, that is, the coproduct free Sumitomo process, which uses organic hydroperoxides that are recycled during the process, and the Hydrogen Peroxide to Propylene Oxide (HPPO) technology.[18,19] This latter

[a] L. K/Bidi, T. Zhang, A. Desjonquères, A. Proust, G. Guillemot
Institut Parisien de Chimie Moléculaire, CNRS, Sorbonne Université, IPCM, 4 place Jussieu, Paris 75005, France
E-mail: geoffroy.guillemot@sorbonne-universite.fr

[b] A. Solé-Daura, J. M. Poblet, J. J. Carbó
Department de Química Física i Inorgànica, Universitat Rovira i Virgili, Marcel·lí Domingo 1, Tarragona 43007, Spain
E-mail: j.carbo@urv.cat

Supporting information for this article is available on the WWW under https://doi.org/10.1002/cctc.202401106

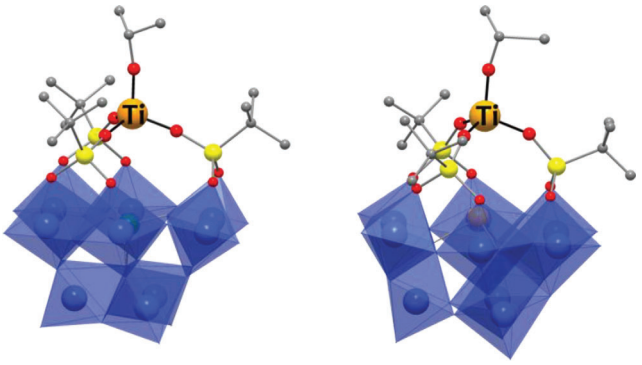

1^{tBu}–Ti 2^{tBu}–Ti

Figure 1. Crystal structures of anions $[\alpha\text{-A-PW}_9O_{34}(t\text{BuSiO})_3\text{Ti}(O i\text{Pr})]^{3-}$ (1^{tBu}-Ti) and $[\alpha\text{-B-SbW}_9O_{33}(t\text{BuSiO})_3\text{Ti}(O i\text{Pr})]^{3-}$ (2^{tBu}-Ti).

is considered as a more environment-friendly and cost-efficient process and its success partly relies on the outstanding catalytic performances of TS-1. These have been extensively associated to the structural peculiarities of the silica lattice, among which hydrophobicity nature and pore size (5–6 Å) of the internal channel system are the most relevant,[20] along with the formation of the reactive titanium-hydroperoxo moiety, either on isolated tetrahedral titanium sites[21,22] or on newly proposed dinuclear sites.[23]

Some of us developed a series of titanium complexes based on silanol functionalized polyoxometalate (*Silox*POMs) derivatives (Figure 1).[24–26] These molecular systems provide a rigid pre-organized set of silanol functionalities that generate a highly constrained coordination site to accommodate titanium (IV) cation in a tetrahedral geometry, as expected in the defective open-lattice sites present in the MFI framework. Most importantly, the use of bulky tert-butyl groups on the silicon atoms creates steric and hydrophobic protection around the metal coordination site. The combination of these two aspects has enabled to present these systems as relevant structural and functional models for titanium silicates, thus able to conduct the epoxidation of allylic alcohols and alkenes through the formation of a postulated titanium (IV)-hydroperoxide [Ti]–(η^2–OOH) active species.[25,26] In the course of our previous studies, we highlighted that despite the apparent similarity between the derivatives described in Figure 1, their activity and selectivity differed as a function of the polyoxotungstic platform used to build the hybrids, namely A-type $[\alpha\text{-A-PW}_9O_{34}]^{9-}$ or B-type $[\alpha\text{-B-SbW}_9O_{33}]^{9-}$. Indeed, the formation of a Ti-peroxo function [Ti]–(η^2–OO) was observed by Raman spectroscopy when using only complex **1^{tBu}-Ti,** and a greater quantity of products from the epoxide ring opening was obtained and identified by NMR spectroscopy. Both of these features can be explained by a shift in the reaction described in Equation 1.[27] However, it seems interesting to understand why the nature of the polyoxotungstic fragment used generates these differences in behavior.

$$[\text{Ti}]-(\text{OOH})+\text{H}_2\text{O} \rightleftarrows [\text{Ti}]-(\text{OO})^- + \text{H}_3\text{O}^+ \quad (1)$$

In order to evaluate how subtle structural divergences strongly impact the behavior of the complexes, we first decided to carry out atomistic molecular dynamic simulations and DFT calculations on the P- and Sb-containing titanium-hydroperoxide complexes in water in order to evaluate the accessibility of the active sites to water molecules and the feasibility of proton transfer to the basic oxygen sites. The results highlighted, as expected, that water is less likely to interact with the titanium hydroperoxide entity embedded in the more confined structure provided by the PW_9 type A structure, but finds easier access to the Ti—O—Si sites, suggesting that they are more susceptible to hydrolysis. This also led us to evaluate the hydrolytic stability of the starting B-type $[XW_9O_{33}(t\text{BuSiOH})_3]^{3-}$ (X = As, Sb) and A-type $[XW_9O_{34}(t\text{BuSiOH})_3]^{n-}$ (X = Si, n = 4; X = P, n = 3) *Silox*POMs to try to conclude on the nature of the epoxidation active species in each case.

2. Results and Discussion

2.1. Relevance of the Catalyst Structures

The titanium derivatives $[PW_9O_{34}(t\text{BuSiO})_3\text{TiO}i\text{Pr}]^{3-}$ (1^{tBu}-Ti) and $[SbW_9O_{33}(t\text{BuSiO})_3\text{TiO}i\text{Pr}]^{3-}$ (2^{tBu}-Ti), prepared as tetrahexyl ammonium salts, are displayed in Figure 1.[25] The former one is obtained from $[PW_9O_{34}]^{9-}$, a A-type $[X(W_3O_{10})(W_2O_8)_3]^{n-}$ usually built around a tetrahedral X heteroatom, such as P(+V) or Si(+IV) in this study, and the second one from $[SbW_9O_{33}]^{9-}$, a B-type $[Y(W_3O_{11})_3]^{9-}$ commonly obtained with pyramidal Y heteroatoms such as Sb(+III) and As(+III).[28] In reaction with tertiobutyl-trichlorosilane, these polyoxotungstic fragments enable to structure a set of three rigid and preorganized silanol functionalities in a C_3 symmetry. One significant difference between $[PW_9O_{34}]^{9-}$ and $[SbW_9O_{33}]^{9-}$ ennea-polyoxotungstic frameworks stems from the size of the lacuna, which is wider in the case of the A-type $[PW_9O_{34}]^{9-}$ derivatives [mean diameter = 7.19 Å] than in the case of the B- type $[SbW_9O_{33}]^{9-}$ structure [mean d = 5.98 Å]. This directly impacts the orientation of the $(-O)_2\text{Si(R)OH}$ groups. As shown in Figure 2, the R groups (*t*Bu in this case) have a more pronounced axial orientation in the case of A-type complex than in the case of B-type complex (angles of 41° and 25° to the mid-plane of the silicon atoms). Consequently, the Si–O–Ti angles are also more obtuse (168° vs. 154°), increasing the π-donation from the oxygen atom and giving less Lewis acidic metal center. Thus, $[SbW_9O_{33}(t\text{BuSiO})_3\text{TiO}i\text{Pr}]^{3-}$ is the best candidate to mimic the environment of the active site in the heterogeneous catalyst (titanium silicates),[29] as it displays very similar geometric parameters, and $[PW_9O_{34}(t\text{BuSiO})_3\text{TiO}i\text{Pr}]^{3-}$ appears to be a less relevant candidate, both for reasons of geometrical constraints and electronics.

2.2. Nuclearity of the Active Site in Contact with Hydrogen Peroxide

The monomeric nature of the active site in the zeolitic catalyst TS-1 was proposed early on by the Italian teams at Enichem (who first prepared TS-1) and found a general consensus amongst the industrial and academic community. Indeed, many spectroscopic

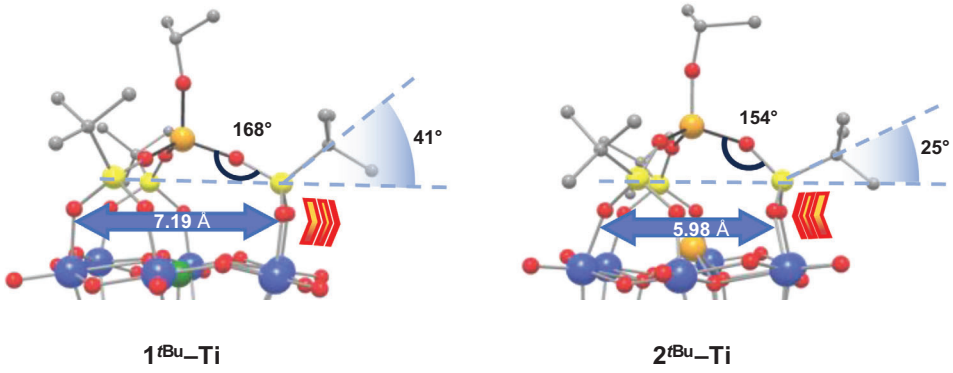

Figure 2. Geometrical differences in 1^{tBu}-Ti and 2^{tBu}-Ti imposed by the lacuna size in the *ennea*-polyoxotungstate $[XW_9O_{34-x}]^{n-}$ frameworks (7.19 versus. 5.98 Å). The chevrons indicate the direction of curvature of the Si–O–W atom sequence, towards the outside of the structure for compound 1^{tBu}-Ti and towards the inside of the structure for compound 2^{tBu}-Ti. Color code: Ti (orange), Si (yellow), W (blue), Sb (orange), P (green), O (red), C (gray).

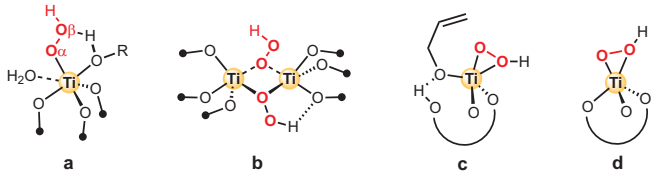

Figure 3. Titanium-hydroperoxide species proposed as active intermediates.

studies demonstrated that Ti atoms are located on isolated sites (only 1%– 2% of the silicon atoms are substituted for Ti atoms in the MFI framework). Recently, Gordon et al. reported evidences that challenge the general assumption of a monomeric active species. In contact to $H_2{}^{17}O_2$, TS-1 samples exhibited a solid-state ^{17}O nuclear magnetic resonance signature that was indicative of the formation of bridging (hydro)peroxo species on dinuclear sites (Figure 3).[11,23] Similar dimeric derivatives, in which the bridging atoms may belong to alkoxide ligands or to μ-oxo or η-peroxo ligands, have been often observed in metalla-siloxane complexes, (used as molecular models for a metal deposited on a silica surface).[30–34] In such derivatives the titanium metal center often increases its coordination shell leading to 5- and 6-coordinated titanium complexes. We early hypothesized that the rigidity of the pre-organized environments in our *Silox*POM systems constrains the metal ion in a strict tetrahedral geometry and postulated that monomeric titanium-hydroperoxide [Ti]-(η^2–OOH) moieties form and act as epoxidizing agents (c and d in Figure 3).

To confirm the nuclearity of these species we completed a series of diffusion-ordered NMR Spectroscopy analysis. The values reported in Table 1 evidence that the reaction product of $[\alpha$-B-$SbW_9O_{33}(RSiO)_3TiOiPr]^{3-}$ (R = *t*Bu, *n*Pr) with aqueous hydrogen peroxide (30% w/w) displays diffusion coefficients values close to the ones measured for the starting monomeric titanium complexes. We should remind at this stage that in contact with water, $[\alpha$-B-$SbW_9O_{33}(tBuSiO)_3TiOiPr]^{3-}$ was reported to form μ-oxo bridged dimer, $[\{\alpha$-B-$SbW_9O_{33}(tBuSiO)_3Ti\}_2O]^{6-}$ (Table 1, entry 2, Figure 4), in which the titanium center remains in a preferred tetrahedral geometry (preliminary X-ray analysis). This was in sharp contrast with the behavior of [α-A-

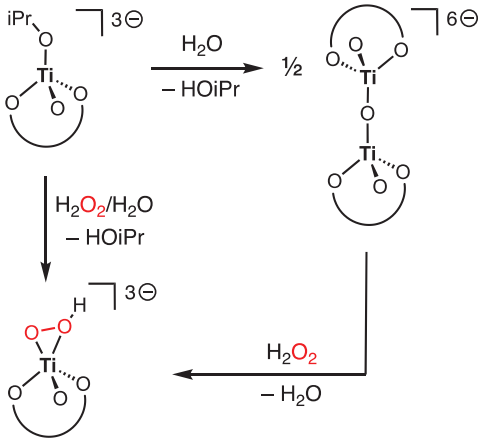

Figure 4. Formation of a dimeric form upon addition of water on 2^{tBu}-Ti and a monomeric form in contact with aqueous hydrogen peroxide.

$PW_9O_{34}(tBuSiO)_3TiOiPr]^{3-}$, for which the hydrolysis reaction of the isopropoxide ligand is only little shifted toward the formation of a monomeric $[PW_9O_{34}(tBuSiO)_3Ti(OH)]^{3-}$, as also revealed by NMR monitoring.[25] This difference is the result of the higher degree of confinement of the metal center in **1^{tBu}-Ti** (as depicted in Figure 2), which prevents dimer formation. Therefore, notwithstanding the presence of water in the hydrogen peroxide solution, a monomeric species preferentially forms, which is thus assigned to the [Ti]–hydroperoxide species, [α-B-$SbW_9O_{33}(tBuSiO)_3Ti(\eta^2$–OOH)]$^{3-}$. The second outcome of this study is that whatever is the size of the substituents at the silicon atom, *t*Bu or *n*Pr, the formation of monomers is always favored (Table 1, entries 3 and 4). In the *Silox*POM hybrid, the trigonal preorganized set of silanol functions constrains the metal ion in a pseudo tetrahedral C_{3v} geometry, which thus limits expansion of its coordination sphere. As far as a realistic correlation with heterogeneous titanium silicates can be drawn, these results emphasize that isolated Ti(IV) in a four coordinated geometry, which is the most common site in the MFI zeolitic frameworks, may form a monomeric [Ti]-hydroperoxide species active in olefin epoxidation upon reaction with H_2O_2.

Table 1. Diffusion coefficients of Ti-*Silox*POMs in presence of H_2O_2.

Entry	Complexes	Diffusion Coefficient (m^2/s)	log(*D*)		Volume Ratio[a)]
1	$(THA)_3[SbW_9O_{33}(t\mathbf{Bu}SiOH)_3]$ (**2^{tBu}**)	$8{,}63.10^{-10}$	−9,06		
2	$(THA)_3[SbW_9O_{33}(t\mathbf{Bu}SiO)_3Ti(OiPr)]$ (**2^{tBu}–Ti**) (monomeric and dimeric mixture)	Monomer	$9{,}21.10^{-10}$	−9,04	1
		Dimer	$7{,}49.10^{-10}$	−9,13	1.85
3	$(THA)_3[SbW_9O_{33}(t\mathbf{Bu}SiO)_3TiOOH]$ (**2^{tBu}–TiOOH**)	$9{,}04.10^{-10}$	−9,04		1.06[a)]
4	$(THA)_3[SbW_9O_{33}(n\mathbf{Pr}SiO)_3TiOOH]$ (**2^{nPr}–TiOOH**)	$9{,}21.10^{-10}$	−9,04		1[a)]

[a)] Ratio are calculated from the value of the diffusion coefficient of the monomeric $(THA)_3[SbW_9O_{33}(tBuSiO)_3Ti(OiPr)]$ considering the following equation derived from the Stokes-Einstein law: $(V_2/V_1) = (D_1/D_2)^3$.

2.3. Access of Water to the Active Sites

Our previous spectroscopic monitoring of catalytic epoxidation of 3-methyl-2-buten-1-ol (an allyl alcohol) using aqueous hydrogen peroxide solution revealed different selectivity when using species **1^{tBu}-Ti** or **2^{tBu}-Ti** as catalysts. ^{31}P and ^{1}H NMR spectroscopy revealed a partial degradation of the phosphotungstate scaffold in $[PW_9O_{34}(t\mathrm{BuSiO})_3TiOiPr]^{3-}$, **$1^{tBu}$-Ti**, and an increased selectivity for 1,2,3-butane-triol, which forms upon ring-opening of the related epoxide (main product).[25] Raman spectroscopy analysis of the same catalytic reaction mixture also indicated the formation of a Ti-peroxide species, Ti-(η^2–O_2). Conversely, when using $[SbW_9O_{33}(t\mathrm{BuSiO})_3TiOiPr]^{3-}$, **$2^{tBu}$-Ti**, as a catalyst, the evolution to the Ti(η^2-O_2) peroxide was not detected by Raman spectroscopy and the expected Ti–(OOH) active species reacted with the allylic alcohol to selectively produce the epoxide. The slightly different behaviour of complex **1^{tBu}-Ti** can tentatively be explained by a proton exchange in the medium, assisted by a water molecule (right shift in Equation (1). This could explain the increased formation of the 1,2,3-butane-triol by an acid-catalyzed opening of the oxirane.

To gain knowledge on the supramolecular implications of the catalyst structure, we carried out atomistic MD simulations (see Experimental Section for details) on the P- and the Sb-containing titanium-hydroperoxide complexes $[PW_9O_{34}(t\mathrm{BuSiO})_3Ti(OOH)]^{3-}$ and $[SbW_9O_{33}(t\mathrm{BuSiO})_3Ti(OOH)]^{3-}$ in water. These simulations served to compare the distribution of water molecules around each complex. Figure 5A compares the radial distribution functions (RDF) between the hydroperoxide hydrogen and the oxygen atom of water molecules of the bulk, computed for **1^{tBu}–Ti** and **2^{tBu}–Ti** catalysts. The shapes of the RDFs anticipate that the Ti-hydroperoxide group of the **2^{tBu}–TiOOH** complex is more prone to interact with the solvent. The derived $H_{TiOOH}\cdots O_{water}$ RDF (Figure 5A, magenta line) shows a sharp peak centered at 1.95 Å, which lays in the distance range of a moderate TiOOH···OH_2 hydrogen bond.[35,36] On the contrary, the RDF computed for **1^{tBu}–Ti** lack this peak but it displays a broader one centered at 3.75 Å that corresponds to a H-bond between a water molecule acting as donor and the β-oxygen of the hydroperoxide. This broad peak also appears for **2^{tBu}–Ti** but it is less important than the first sharper one. The different distribution around both groups is graphically illustrated by the volumetric densities in

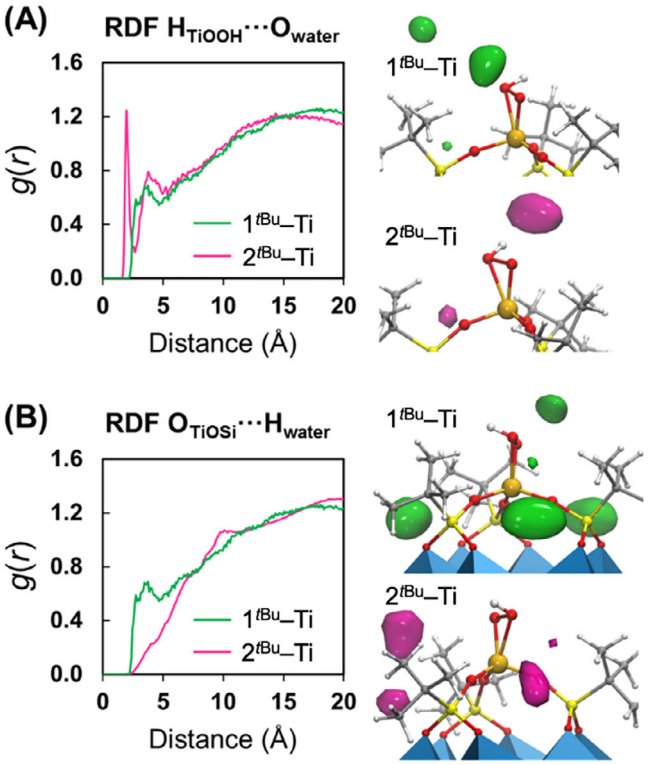

Figure 5. Radial Distribution Functions (RDFs) between the H atom of the TiOOH group and the O atoms of solvent water molecules (A) and between the Ti—O—Si oxygen atoms and the H atoms of solvent water molecules (B) computed from simulations of Ti-hydroperoxide complexes of 1^{tBu}–Ti and 2^{tBu}–Ti in water (green and magenta lines, respectively). Snapshots on the right represent the average volumetric densities of O_{water} atoms within 5 Å of hydroperoxide H atom and that of H_{water} atoms within 5 Å of the Ti—O—Si sites of both catalysts, following the color code defined in the RDFs. Data were averaged over 10 ns with a sampling frequency of 2 ps.

Figure 5A. From this analysis we confirm that the hydroperoxide moiety is less accessible to the solvent in **1^{tBu}–Ti** due to a greater confinement effect (see Figure 2). The geometrical disposition of the *t*Bu groups might also create a hydrophobic environment around the hydroperoxide that hampers the approach of a water molecule. Therefore, the Ti–(OOH) moiety might not be directly the source of protons that catalyze the oxirane ring opening. Accordantly, the free energy change associated to the direct

proton transfer from the Ti–(OOH) to an epoxide molecule was computed to be highly endergonic (>30 kcal·mol^{-1}).

Next, we analyzed the proton transfer step from the Ti–(OOH) moiety to the nearby bridging oxygen atoms (Ti—O—Si in the case of *Silox*POM). Such proton transfer is responsible for the peroxo–hydroperoxo equilibria described in Ti(IV)– and Nb(V)– and Zr(IV)–monosubstituted polyoxometalate structures, in which the peroxo species TM–(η^2-OO) are more stable than hydroperoxo ones or nearly isoenergetic.[37–41] In contrast, for **1^{tBu}–Ti** and **2^{tBu}–Ti** the formation of peroxo complexes Ti–(η^2-OO) is found to be thermodynamically not favorable (+9.3 and +10.2 kcal/mol, respectively). These differences can be attributed to the lower basicity of Ti–O–Si sites in *Silox*POMs compared to Ti–O–W ones in transition-metal substituted polyoxometalates. Also, the barrier for a proton transfer to a Ti–O–Si site in the case of **1^{tBu}–Ti** is lower than that of **2^{tBu}–Ti**, 18.8 versus. 21.5 kcal mol^{-1} (Figures S1 and S2). Nevertheless, the computed free-energy cost for the proton transfer from Ti–(OOH) to Ti–O–Si to form a peroxo species (+9.3 kcal mol in **1^{tBu}–Ti**) does not seem to explain the formation of peroxide **1^{tBu}-Ti-OO$^-$** observed by Raman spectroscopy.

Still, our molecular dynamics simulations also evidenced that water molecules are much more available at the vicinity of the silicon atom in **1^{tBu}–Ti** than in **2^{tBu}–Ti** (Figure 5B). It therefore seems reasonable to envisage a nucleophilic attack at the electrophilic silicon center. This can lead to the protonation of a Si–O–W junction and the formation of a pentavalent silicon intermediate that evolves towards the release of a water molecule using the proton accessible on the Ti-hydroperoxide function (Figure S3). This sequence can hence explain the easiest formation of a Ti–(η^2-OO) entity in **1^{tBu}–Ti** and, overall, corresponds to a proton transfer between Ti-(OOH) and a Si–O–W junction assisted by a water molecule. It is also conceivable that this process is accelerated under the laser beamline when performing resonance Raman spectroscopy.

All combined, experimental observations and calculations reveal the strong impact of the difference in size of the cavity in the A-type $[PW_9O_{34}]^{9-}$ derivatives (7.19 Å) and B-type $[SbW_9O_{33}]^{9-}$ structure (5.98 Å). This obviously affects the orientation of the tertiary butyl groups but, above all, access of the water molecule to the silicon atom is also greatly increased in the A-type derivatives, thus favoring hydrolysis sequences. Moreover, as sketched in Figure 2 by the chevrons, the larger lacuna in type A $[PW_9O_{34}]^{9-}$ has also an influence on the direction of the curvature of the Si–O–W atom sequence. The bridging oxygen atoms point outwards the structure in the A-type based *Silox*POMs, whereas they point inwards the structure in the case of B-type *Silox*POMs. We therefore may expect that they act as privileged sites for an incoming solvated proton in **1^{tBu}-Ti**, resulting in a greater fragility to hydrolysis of the inorganic-organic linkage (Figure 2 and Figure S4) in the presence of protons. In order to confirm that this behavior is a common behavior to A-type based POM hybrids, we prepared additional *Silox*POMs based on both types, $[\alpha$–A–$SiW_9O_{34}(t$BuSiOH$)_3]^{4-}$ and $[\alpha$–B–$AsW_9O_{33}(t$BuSiOH$)_3]^{3-}$ and tested their stability in the presence of water and protons.

2.4. Probing the Stability of the A- and B-Type Hybrid POM

First, stability of the A-type and B-type hybrids was monitored by ^{1}H NMR spectroscopy, in presence of water in acetonitrile solution. Our results evidenced that B–type based hybrids, $[\alpha$–B–$YW_9O_{33}(t$BuSiOH$)_3]^{3-}$ (Y = Sb, As), are less sensitive towards hydrolysis than the A–type analogues, $[\alpha$–A–$XW_9O_{34}(t$BuSiOH$)_3]^{n-}$ (X = Si, n = 4; X = P, n = 3). It is important to note that decomposition only begins at high water concentrations: [H_2O] = 6.5 M; [SiloxPOM] = 0.013 M (500:1 ratio). The decomposition is mostly evidenced by the appearance of tiny secondary peaks around –15 ppm in ^{31}P NMR (Figures S5 and S6). Hybrid POM hydrolysis is drastically enhanced by the addition of acids. *Silox*POMs based on type B remain stable up to the addition of 10 equivalents of protons, whereas *Silox*POMs based on type A appear less stable, with a clear difference between the Si and P derivatives. In the case of the B–type based hybrids, $[\alpha$–B–$YW_9O_{33}(t$BuSiOH$)_3]^{3-}$ (Y = Sb, As), as the amount of HCl increases (>20 equivalents), we observed by ^{1}H NMR a partial degradation of the hybrid POM corresponding to several new peaks at 1.18 and 0.95 ppm (Figure S7). In the case of the A–type analogues $[\alpha$–A–$XW_9O_{34}(t$BuSiOH$)_3]^{n-}$ (X = Si, n = 4; X = P, n = 3), the difference between the Si and P derivatives can be attributed to the difference in overall charge, 4- and 3- respectively, thus increasing basicity. Indeed, the addition of two equivalents of HCl to a solution of $[\alpha$–A–$SiW_9O_{34}(t$BuSiOH$)_3]^{4-}$ in acetonitrile already led to a new signal at 0.92 ppm, attributed to a species in which a Si–O–W has been cleaved (Figure S8).[42] In the case of $[\alpha$–A–$PW_9O_{34}(t$BuSiOH$)_3]^{3-}$, the hybrid remained stable until the addition of 10 equivalents of HCl. In these conditions, we observed the growth of new signals at 1.05 ppm by ^{1}H NMR. ^{31}P NMR monitoring highlighted new signals at -14.5 ppm, with low intensity compared to the signal of the hybrid complex at -16.9 ppm (Figure S9). Overall stability therefore follows this order: $[\alpha$–B–$SbW_9O_{33}(t$BuSiOH$)_3]^{3-} \sim [\alpha$–B–$AsW_9O_{33}(t$BuSiOH$)_3]^{3-} > [\alpha$–A–$PW_9O_{34}(t$BuSiOH$)_3]^{3-} > [\alpha$–A–$SiW_9O_{34}(t$BuSiOH$)_3]^{4-}$.

While dealing with the use of POMs as oxidation catalysts, one should bear in mind the solvolytic instability of some Keggin type structures in aqueous hydrogen peroxide solutions.[43,44] In the case of hybrids of POMs, both base- and acid-catalyzed hydrolysis may lead to the release of silanol arms and the generation of *cis*-W(=O)$_2$ units that may react with H_2O_2. Similarly, degradation of the oxotungstate core may also proceed through the release of $\{WO_2\}^{2+}$ species, which can further react with H_2O_2 to form Mimoun-[45] or Venturello-like species,[46] both active in olefin epoxidation.[47] In this context, oxidation reaction goes through well-known d^0-metal/peroxide chemistry; a metal-oxo function, W = O, reacts with H_2O_2 to form a metal-peroxide W(η^2–O_2) and water.[48] We observed that in the presence of H_2O_2 (as a 30 wt % aqueous solution, up to 60 eq), *Silox*POMs from type B structures remained stable as evidenced by ^{1}H NMR (Figure S10). Conversely, the stability of *Silox*POMs from type A structures was lower and ^{31}P NMR monitoring of $[\alpha$–A–$PW_9O_{34}(t$BuSiOH$)_3]^{3-}$ revealed the formation of a species spectroscopically similar to that described by Ishii and Venturello (Figures S11 and S12).

Table 2. Epoxidation of olefins catalyzed by $[\alpha\text{–B–SbW}_9O_{33}(t\text{BuSiO})_3\text{TiO}i\text{Pr}]^{3-}$ using either an aqueous or an anhydrous solution of hydrogen peroxide.[a]

Entry	H_2O_2	Olefin	Conv. (%)[b]	Selectivity for Epoxidation (%)[c]
1	H_2O_2/H_2O (30% w/w)	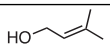	96	87
2	H_2O_2/CH_3CN (*anhy.*)		95	92
3	H_2O_2/H_2O (30% w/w)		<5	-[d]
4	H_2O_2/CH_3CN (*anhy.*)		37	>95[e]

[a] All reactions were carried out in acetonitrile solution at room temperature (20 °C) with a catalyst:olefin:H_2O_2 ration of 1:60:120; $[H_2O_2]_0$ = 0.16 M for aqueous solution and 0.2 M for anhydrous solution.
[b] Conversion is based on the minimum concentration of olefin that can be reached if all hydrogen peroxide is used for the oxidization reaction, after 4 h of reaction.
[c] Major side products are triol (7%) and aldehyde (3%).
[d] Traces of side products are not detected, hydrogen peroxide decomposition was the only reaction observed.
[e] No other products were observed by NMR.

NMR spectroscopy is not precise enough to detect very small quantities of impurities, and apparent stability can be deceptive if the tiny, degraded portion turns out to be sufficiently active in catalysis. We therefore use the epoxidation of allylic alcohols to probe the effective stability of the *Silox*POMs. When using *non-metalated* A-type $[\alpha\text{–A–PW}_9O_{34}(t\text{BuSiOH})_3]^{3-}$ and $[\alpha\text{–A–SiW}_9O_{34}(t\text{BuSiOH})_3]^{4-}$, thus expected to be catalytically unactive, a significant conversion to epoxide was nevertheless observed especially in the first 4 hours of reaction. Conversely, when using B-type $[\alpha\text{–B–SbW}_9O_{33}(t\text{BuSiOH})_3]^{3-}$ and $[\alpha\text{–B–AsW}_9O_{33}(t\text{BuSiOH})_3]^{3-}$ no significant conversion to epoxide was observed especially for the first 4 hr, and then conversion started only very smoothly (Figure S13). Over these first 4 hr, H_2O_2 concentration also did not decrease, showing that the B-type POMs were neither active for hydrogen peroxide decomposition. These results correlate perfectly with stability studies conducted in slightly acidic conditions.

2.5. Key Role of Water

To get an insight into the effect of water on the activity and selectivity of epoxidation reaction catalyzed by the Ti-*Silox*POM complexes, we used an anhydrous solution of hydrogen peroxide in acetonitrile, and compared the results to the ones obtained when using an aqueous solution of hydrogen peroxide. When the substrate used is an allylic alcohol, the absence of water does not really improve the catalytic activity of the B-type $[\alpha\text{–B–SbW}_9O_{33}(t\text{BuSiO})_3\text{TiO}i\text{Pr}]^{3-}$ complex, although selectivity for epoxide was increased (Table 2, entries 1 and 2). We attributed this result to the fact that allylic alcohol binds the titanium center in the catalytic resting state and therefore acts as a *protecting group*, preventing H_2O_2 decomposition and favoring the O-atom transfer in an inner-sphere pathway (species c in Figure 3). Surprisingly, in the case of cyclohexene, an unfunctionalized olefin that does not bind the titanium, the effect of absence of water on the results of epoxidation catalysis was remarkable (Table 2, entries 3 and 4). Although conversion of H_2O_2 in unproductive ways was observed when using an aqueous hydrogen peroxide solution, the epoxidation reaction becomes competitive when an anhydrous hydrogen peroxide solution was used (entries 3 and 4). The difference in reactivity between allyl alcohol and cyclohexene reflects the different nature of the reaction pathways – *inner-sphere* vs *outer-sphere* mechanism – and the active species involved (c and d in Figure 3).[25,26]

These latest results clearly show that water is involved in the decomposition of hydrogen peroxide by titanium complexes. In its absence, epoxidation of non-functionalized olefins becomes a competitive pathway, and the activity of titanium derivatives of SiloxPOMs built on type B can be demonstrated.

3. Conclusion

*Silox*POMs $(THA)_n[\alpha\text{–A–XW}_9O_{34}(t\text{BuSiOH})_3]$ and $(THA)_n[\alpha\text{–B–YW}_9O_{33}(t\text{BuSiOH})_3]$ have proved to be relevant ligands for modeling the tris-silanol coordination environment of tetrahedral defective open-lattice sites $[(\equiv\text{Si}-\text{O})_3\text{Ti(OH)}]$ that are present in titanium silicates. However, there are significant differences between the two hybrid systems. Whereas *Silox*POM built on the A–type structures allow to generate a higher cavity effect around the tris-silanol coordination site (and thus a more *hydrophobic* environment) it exposes the W–O–Si linkage to acid hydrolysis. This is the result of the wider lacuna in A type $[PW_9O_{34}]^{9-}$ derivatives, which impacts the orientation of the $(-O)_2\text{Si(R)OH}$ groups, with R groups pointing in a more axial orientation than in B-type derivatives. As a direct consequence, the Si–O–W oxygen atoms point *outwards* the structure and act therefore as privileged sites for an incoming solvated proton, whereas in B-type *Silox*POMs the oxygen atoms point *inwards* the structure. The influence of these structural features on the accessibility of protons/water molecules to relevant sites of the hybrid structures has been analyzed by theoretical methods. Atomistic Molecular Dynamics simulations support a more solvent-accessible nature of bridging oxygens connecting catalytic centers to polyoxotungstate frameworks in A-type structures, which might be linked to their lower stability towards hydrolysis compared to the B-type *Silox*POM derivatives. Also, DFT calculations indicate that A-type *Silox*POMs are more likely to undergo protonation at a Ti-O-Si site, thus weakening

Ti-POM linkages. Jointly, these are the key points that enable (THA)$_3$[α–B–SbW$_9$O$_{33}$(*t*BuSiO)$_3$Ti(O*i*Pr)] to behave as relevant models for crystalline microporous titanium silicates. Our DOSY NMR studies and catalytic tests carried out with anhydrous hydrogen peroxide confirmed that isolated site can be an active site for epoxidation catalysis. Moreover, through experimental data and theoretical analysis, this study offers detailed insights into the design and optimization of titanium-based catalysts for efficient and selective oxidation reactions.

4. Experimental Section

4.1. Materials and Methods

The lacunary polyoxotungstate Na$_9$[α-B-SbW$_9$O$_{33}$], K$_9$[α-A-PW$_9$O$_{34}$], Na$_9$[α-B-AsW$_9$O$_{33}$] and Na$_{10}$[α-A-SiW$_9$O$_{34}$] were prepared as reported in the literature.[49,50] Their silanol derivatives (*n*-Hex$_4$N)$_3$[(α-A-PW$_9$O$_{34}$)(*t*BuSiOH)$_3$] (**1^{tBu}**), (*n*-Hex$_4$N)$_3$[(α-B-SbW$_9$O$_{33}$)(*R*SiOH)$_3$] (**2^{tBu}** R = *t*Bu, **2^{nPr}** R = *n*Pr), (*n*-Hex$_4$N)$_3$[(α-B-AsW$_9$O$_{33}$)(*t*BuSiOH)$_3$] and (*n*-Bu$_4$N)$_4$[(α-A-SiW$_9$O$_{34}$)(*t*BuSiOH)$_3$] were prepared according to reported procedures or modified ones (*vide infra*).[51,25] The titanium complexes (*n*-Hex$_4$N)$_3$[(α-A-PW$_9$O$_{34}$)(*t*BuSiO)$_3$Ti(O*i*Pr)] (**1^{tBu}-Ti**), (*n*-Hex$_4$N)$_3$[(α-B-SbW$_9$O$_{33}$)(*n*PrSiO)$_3$Ti(O*i*Pr)] (**2^{nPr}-Ti**) and (*n*-Hex$_4$N)$_3$[(α-B-SbW$_9$O$_{33}$)(*t*BuSiO)$_3$Ti(O*i*Pr)] (**2^{tBu}-Ti**) were prepared as reported in the literature.[25,26] All manipulations were conducted under an inert atmosphere using standard Schlenk techniques and a glovebox with purification system. Tetrahydrofuran and acetonitrile were dried using solvent purification systems or by distillation under argon from appropriate drying agents. All solvents, including deuterated acetonitrile, were then degassed by several freeze–pump–thaw cycles and stored over activated molecular sieves. Titanium tetra-isopropoxide, Ti(OiPr)$_4$, hydrogen peroxide (30 wt % in H$_2$O) and olefins were purchased from Sigma, Alfa, or Acros and used as received. Anhydrous hydrogen peroxide solution was prepared from urea-H$_2$O$_2$ adduct as reported above. ^{1}H NMR, ^{31}P NMR, ^{29}Si NMR spectra were obtained at room temperature in 5 mm o.d. tubes on a Bruker Avancell 300 spectrometer equipped with a QNP probehead or on a Bruker AvancellI 600 spectrometer equipped with a BBFO probehead. For ^{1}H, chemical shifts are referenced with respect to tetramethylsilane by using the solvent signals as secondary standard. For ^{31}P{^{1}H}, chemical shifts were measured by the substitution method and are given with respect to 85% H$_3$PO$_4$. Elemental analyses were performed at ICSN–CNRS, Gif-sur-Yvette, France.

4.1.1. Synthesis of THA$_3$[AsW$_9$O$_{33}$(tBuSiOH)$_3$]

Na$_9$[AsW$_9$O$_{33}$] (3.0 g, 1.12 mmol) and 1.951 g [(C$_6$H$_{13}$)$_4$N]Br (1.95 g, 4.489 mmol) were placed in a dried Schlenk tube and, under argon atmosphere, freshly distilled CH$_3$CN (30 mL) was added. The suspension was first cooled to 0 °C for 0.5 h, then *t*BuSiCl$_3$ (0.65 g, 3.37 mmol) was added, and vigorous stirring was maintained overnight at 0 °C. The suspension was allowed to warm to room temperature, and then the solid was filtered off (mixture of NaCl, NaBr, and unreacted reactants). The solution was then evaporated to ca. 15 mL and layered with diethyl ether to achieve crystals, which was washed with diethyl ether, and dried under vacuum. Yield: 2.26 g (55.5%). Anal. Calc for C$_{84}$H$_{186}$N$_3$O$_{36}$AsSi$_3$W$_9$ (3628.11): C, 27.81; H, 5.17; N, 1.16. Found: C 27.72, H 5.17, N 0.92. ^{1}H NMR (CD$_3$CN, 400 MHz, 300 K) δ, ppm: 3.14 (m, 24H, NC*H*$_2$ THA), 1.65 (m, 24H, NCH$_2$C*H*$_2$ THA), 1.35 (m, 72H, (C*H*$_2$)$_3$CH$_3$ THA), 1.15 (s, 27H, CH$_3$ *t*BuSi), 0.91 (t, $^3J_{H,H}$ = 6.9 Hz; 36H, CH$_2$C*H*$_3$ THA). ^{29}Si NMR (CD$_3$CN, 79.5 MHz, 300 K) δ, ppm: −43.83 (s).

4.1.2. Synthesis of TBA$_4$[SiW$_9$O$_{34}$(tBuSiOH)$_3$]

α-A-Na$_{10}$[SiW$_9$O$_{34}$] (2.08 g, 0.78 mmol) and [(C$_4$H$_9$)$_4$N]Br (1.13 g, 3.443 mmol) were placed in a dried Schlenk tube, and, under argon atmosphere, freshly distilled CH$_3$CN (20 mL) was added. The suspension was first cooled to 0 °C for 0.5 h, then *t*BuSiCl$_3$ (0.63 g, 3.11 mmol) was added, and vigorous stirring was maintained overnight at 0 °C. The suspension was allowed to warm to room temperature, and the solid was filtered off (mixture of NaCl, NaBr, and unreacted reactants). The solution was then evaporated, and the crude was washed with pentane and water. Crystals were obtained from dimethyl formamide solution and dried under vacuum. Yield: 1 g (37%). Anal. Calc for C$_{76}$H$_{174}$N$_4$O$_{37}$Si$_4$W$_9$ (3503.10): C, 26.06; H, 5.01; N, 1.60; Found: C, 24.96; H, 4.71; N, 1.68. ^{1}H NMR (CD$_3$CN, 400 MHz, 300 K) δ, ppm: 3.14 (m, 32H, NC*H*$_2$ TBA), 1.63 (m, 32H, NCH$_2$C*H*$_2$ TBA), 1.41 (m, 32H, C*H*$_2$CH$_3$ TBA), 0.95 (s, 27H, CH$_3$ *t*BuSi), 0.98 (t, $^3J_{H,H}$ = 7.28 Hz; 48H, CH$_2$C*H*$_3$ TBA). ^{29}Si NMR (CD$_3$CN, 79.5 MHz, 300 K) δ, ppm: −47.11 (s), −88.38 (s).

4.1.3. Anhydrous H$_2$O$_2$ solution in acetonitrile (~0.2 M)

Urea-hydrogen peroxide adduct (0.4 mmol) was placed in a Schlenk tube under argon atmosphere. 2 mL of anhydrous acetonitrile (or deuterated acetonitrile) were added, and the suspension was stirred vigorously at room temperature for 3 hr. The solution was cooled at 5°C overnight and solid urea was then filtered under argon atmosphere. The solution was used as prepared. The concentration of the solution was determined by titration with an aqueous solution of KMnO$_4$ at 0.01 M in presence of sulfuric acid (~1 M).

4.1.4. DOSY ^{1}H NMR

All the measurements were done under strictly the same conditions (NMR apparatus, concentration, temperature) to allow comparison between the diffusion coefficients values. *Silox*POM (0.0018 mmol, 1 equiv.) was dissolved in anhydrous CD$_3$CN, in an NMR tube equipped with a screw cap and under argon atmosphere. Commercial aqueous hydrogen peroxide (0.035 mmol) was added to the solution.

4.1.5. NMR monitoring – olefin epoxidation

Ti-*Silox*POM (1.3 mmol, 1 equiv.) and olefin (160 mmol, 120 equiv.) were placed in an NMR test tube with a screw cap, under argon atmosphere. Anhydrous hydrogen peroxide solution in CD$_3$CN (60 equiv) or CD$_3$CN and commercial aqueous hydrogen peroxide (60 equiv.) were added to the mixture. The reaction was followed by ^{1}H NMR over time.

4.2. Computational Details

DFT calculations were carried out using the Gaussian09 (revision A02) quantum chemistry package,[52] and adopting the B3LYP[53–55] exchange-correlation function. Ti, W and Sb centers were described by the LANL2DZ[56] basis set and associated pseudopotentials and the Pople-type 6–31G basis set[57–59] was used for the remaining atoms. Solvent effects of acetonitrile were included in all the calculations using IEF-PCM model[60] as implemented in Gaussian09. Normal mode analysis confirmed the stationary point nature of

both minima- and transition-state structures. Gibbs free energies were calculated at the standard state of 1 mol·L^{-1} and 25 °C. A data set of the most representative structures from the reported mechanisms are available in the ioChem-BD repository[61] and can be accessed via the following link: 10.19061/iochem-bd-2-70.

Molecular Dynamics (MD) simulations were performed using the GROMACS 4.5.4 code[62–64] and the Amber 99 force field.[65] Force field parameters for POM structures were retrieved from previous works,[66,67] whereas the set of Lennard-Jones parameters for Sb and Ti were obtained from the UFF force field. Water molecules were described by the TIP3P model. Atomic charges were obtained following the procedure outlined by Bonet-Ávalos and coworkers.[66,67] For the simulations, either **1^{tBu}—Ti** or **2^{tBu}—Ti** were embedded into cubic, 3D-periodic water solvent cages of 40.2680^3 Å or 40.1196^3, respectively, including 3 Na^+ counter cations to compensate the charge. An interatomic distance cut-off of 14 Å was used for both van der Waals and for Coulombic interactions. Long-range electrostatics were corrected using the particle-particle mesh Ewald (PME) summation method.[68] Following 10'000 steps of energy minimization and 250 ps of NVT equilibration, both systems were simulated for 500 ps of NPT conditions to adjust the box dimensions and hence, the density. Finally, after 250 ps of NVT equilibration, both systems were simulated for 10 ns under the NVT ensemble. Newton equations of motion were integrated using the leap-frog algorithm[69] with a time step of 1 fs. Bonds containing hydrogen atoms were constraint using the LINCS algorithm.[70] The temperature was controlled by the velocity rescaling algorithm[71] with a relaxation time of 0.1 ps. For equilibrations within the isothermal-isobaric (NPT) ensemble, the system was coupled to the Berendsen algorithm[72] at 1 bar. Data were collected from the trajectories every 2 ps.

Acknowledgments

French Ministry of Higher Education and Research and the Sorbonne University CSC program are acknowledged for PhD grants to L. K/B. and T.Z. GG also acknowledges the CNRS (International Emerging Action grant 00551) for generous support. We also thank grant PID2021-128128NB-I00, funded by MCIN/AEI/10.13039/501100011033 and by "ERDF A way of making Europe", and the Generalitat de Catalunya (2021SGR00110). A. S.-D. also acknowledges the Spanish Ministry of Universities and the European Union – Next Generation EU for their financial support through a Margarita Salas grant.

Keywords: Catalyst stability · DFT and MD simulations · Hydrogen peroxide · Polyoxotungstates · Titanium

[1] R. A. Sheldon, I. W. C. E. Arends, U. Hanefeld, *Green Chemistry and Catalysis*, Wiley-VCH, Weinheim, **2007**, pp. 133–221.
[2] I. W. C. E. Arends, V. Conte, G. Licini, *Innovative Catalysis in Organic Synthesis*, John Wiley & Sons, Ltd, **2012**, pp. 77–102.
[3] R. A. Sheldon, J. K. Kochi, *Metal-Catalyzed Oxidations of Organic Compounds*, Academic Press, New York, **1981**.
[4] R. Ciriminna, L. Albanese, F. Meneguzzo, M. Pagliaro, *ChemSusChem* **2016**, *9*, 3374–3381.
[5] *Catalytic Oxidations with Hydrogen Peroxide as Oxidant* (Ed: G. Strukul), Kluwer Academic Publishers, Netherlands, **1992**.
[6] B. S. Lane, K. Burgess, *Chem. Rev.* **2003**, *103*, 2457–2474.
[7] R. A. Baglia, J. P. T. Zaragoza, D. P. Goldberg, *Chem. Rev.* **2017**, *117*, 13320–13352.
[8] K. Matsumoto, Y. Sawada, B. Saito, K. Sakai, T. Katsuki, *Angew. Chem., Int. Ed.* **2005**, *44*, 4935–4939.
[9] S. Kondo, K. Saruhashi, K. Seki, K. Matsubara, K. Miyaji, T. Kubo, K. Matsumoto, T. Katsuki, *Angew. Chem., Int. Ed.* **2008**, *47*, 10195–10198.
[10] A. Berkessel, T. Günther, Q. Wang, J.-M. Neudörfl, *Angew. Chem., Int. Ed.* **2013**, *52*, 8467–8471.
[11] H. Engler, M. Lansing, C. P. Gordon, J.-M. Neudörfl, M. Schäfer, N. E. Schlörer, C. Copéret, A. Berkessel, *ACS Catal.* **2021**, 3206–3217.
[12] *Comprehensive Asymmetric Catalysis* (Eds: E. N. Jacobsen, A. Pfaltz, H. Yamamoto), Springer-Verlag, Berlin Heidelberg, **1999**.
[13] G. Perego, G. Bellussi, C. Corno, M. Taramasso, F. Buonomo, A. Esposito, *Studies in Surface Science and Catalysis*, Vol. *28*, **1986**, pp. 129–136.
[14] M. G. Clerici, G. Bellussi, U. Romano, *J. Catal.* **1991**, *129*, 159–167.
[15] I. W. C. E. Arends, R. A. Sheldon, M. Wallau, U. Schuchardt, *Angew. Chem. Int. Ed. Engl.* **1997**, *36*, 1144–1163.
[16] O. A. Kholdeeva, *Catal. Sci. Technol.* **2014**, *4*, 1869–1889.
[17] M. G. Clerici, P. Ingallina, *J. Catal.* **1993**, *140*, 71–83.
[18] S. B. Shin, D. Chadwick, *Ind. Eng. Chem. Res.* **2010**, *49*, 8125–8134.
[19] V. Russo, R. Tesser, E. Santacesaria, M. Di Serio, *Ind. Eng. Chem. Res.* **2013**, *52*, 1168–1178.
[20] T. Tatsumi, *Modern Heterogeneous Oxidation Catalysis: Design, Reactions and Characterization* (Ed: N. Mizuno), John Wiley & Sons, Inc **2009**, pp. 125–155.
[21] M. G. Clerici, M. E. Domine, in *Liquid Phase Oxidation via Heterogeneous Catalysis: Organic Synthesis and Industrial Applications*, John Wiley & Sons, Inc **2013**, p. 21.
[22] M. G. Clerici, *Kinet. Catal.* **2015**, *56*, 450–455.
[23] C. P. Gordon, H. Engler, A. S. Tragl, M. Plodinec, T. Lunkenbein, A. Berkessel, J. H. Teles, A.-N. Parvulescu, C. Copéret, *Nature* **2020**, *586*, 708–713.
[24] G. Guillemot, E. Matricardi, L.-M. Chamoreau, R. Thouvenot, A. Proust, *ACS Catal.* **2015**, *5*, 7415–7423.
[25] T. Zhang, L. Mazaud, L.-M. Chamoreau, C. Paris, A. Proust, G. Guillemot, *ACS Catal.* **2018**, *8*, 2330–2342.
[26] A. Solé-Daura, T. Zhang, H. Fouilloux, C. Robert, C. M. Thomas, L.-M. Chamoreau, J. J. Carbó, A. Proust, G. Guillemot, J. M. Poblet, *ACS Catal.* **2020**, *10*, 4737–4750.
[27] F. Bonino, A. Damin, G. Ricchiardi, M. Ricci, G. Spanò, R. D'Aloisio, A. Zecchina, C. Lamberti, C. Prestipino, S. Bordiga, *J. Phys. Chem. B.* **2004**, *108*, 3573–3583.
[28] R. Contant, G. Herve, *Rev. Inorg. Chem.* **2011**, *22*, 63–112.
[29] J. Dong, H. Zhu, Y. Xiang, Y. Wang, P. An, Y. Gong, Y. Liang, L. Qiu, A. Zheng, X. Peng, M. Lin, G. Xu, Z. Guo, D. Chen, *J. Phys. Chem. C* **2016**, *120*, 20114–20124.
[30] R. Murugavel, A. Voigt, M. G. Walawalkar, H. W. Roesky, *Chem. Rev.* **1996**, *96*, 2205–2236.
[31] M. Crocker, R. H. M. Herold, M. Crocker, A. G. Orpen, *Chem. Commun.* **1997**, 2411–2412.
[32] R. Duchateau, *Chem. Rev.* **2002**, *102*, 3525–3542.
[33] E. A. Quadrelli, J.-M. Basset, *Coord. Chem. Rev.* **2010**, *254*, 707–728.
[34] A. J. Ward, R. Lesic, A. F. Masters, T. Maschmeyer, *Proc Math Phys Eng Sci* **2012**, *468*, 1968–1984.
[35] G. A. Jeffrey, *An Introduction to Hydrogen Bonding*, Oxford University Press, **1997**.
[36] T. Steiner, *Angew. Chem. Intl. Ed.* **2002**, *41*, 48–76.
[37] N. S. Antonova, J. J. Carbó, U. Kortz, O. A. Kholdeeva, J. M. Poblet, *J. Am. Chem. Soc.* **2010**, *132*, 7488–7497.
[38] N. V. Maksimchuk, G. M. Maksimov, V. Yu. Evtushok, I. D. Ivanchikova, Y. A. Chesalov, R. I. Maksimovskaya, O. A. Kholdeeva, A. Solé-Daura, J. M. Poblet, J. J. Carbó, *ACS Catal.* **2018**, *8*, 9722–9737.
[39] P. Jiménez-Lozano, I. Y. Skobelev, O. A. Kholdeeva, J. M. Poblet, J. J. Carbó, *Inorg. Chem.* **2016**, *55*, 6080–6084.
[40] N. V. Maksimchuk, I. D. Ivanchikova, G. M. Maksimov, I. V. Eltsov, V. Y. Evtushok, O. A. Kholdeeva, D. Lebbie, R. J. Errington, A. Solé-Daura, J. M. Poblet, J. J. Carbó, *ACS Catal.* **2019**, *9*, 6262–6275.
[41] N. V. Maksimchuk, V. Y. Evtushok, O. V. Zalomaeva, G. M. Maksimov, I. D. Ivanchikova, Y. A. Chesalov, I. V. Eltsov, P. A. Abramov, T. S. Glazneva, V. V. Yanshole, O. A. Kholdeeva, R. J. Errington, A. Solé-Daura, J. M. Poblet, J. J. Carbó, *ACS Catal.* **2021**, *11*, 10589–10603.
[42] L. Alloul, N. Ammari, C. R. Mayer, A. Mazeaud, R. Thouvenot, *J. Chim. Phys. Pcb.* **1998**, *95*, 289–294.

[43] P. J. Domaille, *Inorg. Synth.* **1990**, *27*, 96.
[44] L. Salles, C. Aubry, R. Thouvenot, F. Robert, C. Doremieux-Morin, G. Chottard, H. Ledon, Y. Jeannin, J. M. Bregeault, *Inorg. Chem.* **1994**, *33*, 871–878.
[45] H. Mimoun, *Angew. Chem.-Int. Edit.* **1982**, *21*, 734–750.
[46] C. Venturello, R. D'Aloisio, J. C. J. Bart, M. Ricci, *J. Mol. Catal.* **1985**, *32*, 107–110.
[47] J.-M. Brégeault, M. Vennat, S. Laurent, J.-Y. Piquemal, Y. Mahha, E. Briot, P. C. Bakala, A. Atlamsani, R. Thouvenot, *J. Mol. Catal. A: Chem.* **2006**, *250*, 177–189.
[48] K. Kamata, M. Kotani, K. Yamaguchi, S. Hikichi, N. Mizuno, *Chem. - Eur. J.* **2007**, *13*, 639–648.
[49] C. Tourne, A. Revel, G. Tourne, M. Vendrell, *C. R. Acad. Sci., Ser. C.* **1973**, *277*, 643–645.
[50] A. Tézé, G. Hervé, in *Inorganic Syntheses*, Vol. *27*, pp. 85–96.
[51] A. Mazeaud, N. Ammari, F. Robert, R. Thouvenot, *Angew. Chem., Int. Ed.* **1996**, *35*, 1961–1964.
[52] M. J. Frisch, G. W. Trucks, H. B. Schlegel, G. E. Scuseria, M. A. Robb, J. R. Cheeseman, G. Scalmani, V. Barone, G. A. Petersson, H. Nakatsuji, X. Li, M. Caricato, A. V. Marenich, J. Bloino, B. G. Janesko, R. Gomperts, B. Mennucci, H. P. Hratchian, J. V. Ortiz, A. F. Izmaylov, J. L. Sonnenberg, F. Ding Williams, F. Lipparini, F. Egidi, J. Goings, B. Peng, A. Petrone, T. Henderson, D. Ranasinghe, V. G. Zakrzewski, et al., Gaussian, Inc., Wallingford CT, **2016**.
[53] C. Lee, W. Yang, R. G. Parr, *Phys. Rev. B.* **1988**, *37*, 785–789.
[54] A. D. Becke, *J. Chem. Phys.* **1993**, *98*, 5648–5652.
[55] P. J. Stephens, F. J. Devlin, C. F. Chabalowski, M. J. Frisch, *J. Phys. Chem.* **1994**, *98*, 11623–11627.
[56] P. J. Hay, W. R. Wadt, *J. Chem. Phys.* **1985**, *82*, 299–310.
[57] W. J. Hehre, R. Ditchfield, J. A. Pople, *J. Chem. Phys.* **1972**, *56*, 2257–2261.
[58] P. C. Hariharan, J. A. Pople, *Theoret. Chim. Acta.* **1973**, *28*, 213–222.
[59] M. M. Francl, W. J. Pietro, W. J. Hehre, J. S. Binkley, M. S. Gordon, D. J. DeFrees, J. A. Pople, *J. Chem. Phys.* **1982**, *77*, 3654–3665.
[60] E. Cancès, B. Mennucci, J. Tomasi, *J. Chem. Phys.* **1997**, *107*, 3032–3041.
[61] M. Álvarez-Moreno, C. de Graaf, N. López, F. Maseras, J. M. Poblet, C. Bo, *J. Chem. Inf. Model.* **2015**, *55*, 95–103.
[62] B. Hess, C. Kutzner, D. van der Spoel, E. Lindahl, *J. Chem. Theory Comput.* **2008**, *4*, 435–447.
[63] D. Van Der Spoel, E. Lindahl, B. Hess, G. Groenhof, A. E. Mark, H. J. C. Berendsen, *J. Comput. Chem.* **2005**, *26*, 1701–1718.
[64] H. J. C. Berendsen, D. van der Spoel, R. van Drunen, *Comput. Phys. Commun.* **1995**, *91*, 43–56.
[65] J. Wang, P. Cieplak, P. A. Kollman, *J. Comp. Chem.* **2000**, *21*, 1049–1074.
[66] X. López, C. Nieto-Draghi, C. Bo, J. B. Avalos, J. M. Poblet, *J. Phys. Chem. A.* **2005**, *109*, 1216–1222.
[67] F. Leroy, P. Miró, J. M. Poblet, C. Bo, J. Bonet Ávalos, *J. Phys. Chem. B.* **2008**, *112*, 8591–8599.
[68] T. Darden, D. York, L. Pedersen, *J. Chem. Phys.* **1993**, *98*, 10089–10092.
[69] R. W. Hockney, S. P. Goel, J. W. Eastwood, *J. Comp. Phys.* **1974**, *14*, 148–158.
[70] B. Hess, H. Bekker, H. J. C. Berendsen, J. G. E. M. Fraaije, *J. Comp. Chem.* **1997**, *18*, 1463–1472.
[71] G. Bussi, D. Donadio, M. Parrinello, *J. Chem. Phys.* **2007**, *126*, 014101.
[72] H. J. C. Berendsen, J. P. M. Postma, W. F. van Gunsteren, A. DiNola, J. R. Haak, *J. Chem. Phys.* **1984**, *81*, 3684–3690.

Manuscript received: June 27, 2024
Revised manuscript received: September 09, 2024
Accepted manuscript online: September 10, 2024
Version of record online: September 18, 2024